Supplementary Data: Turnover modulates the need for a cost of resistance in adaptive therapy

Maximilian Strobl, Jeffrey West, Yannick Viossat, Mehdi Damaghi,
Mark Robertson-Tessi, Joel Brown, Robert Gatenby,
Philip Maini, Alexander Anderson

November 5, 2020

S1 *In vitro* spheroid experiments

S1.1 Sensitive and resistant cell culture

MCF7 cells were acquired from American Type Culture Collection (ATCC, Manassas, VA, 2007–2010) and were maintained in RPMI 1640 (Life Technologies) supplemented with 10% FBS (HyClone Laboratories). Cells were tested for mycoplasma contamination and authenticated using short tandem repeat (STR) DNA typing according to ATCC guidelines. To establish stable cell lines expressing GFP and RFP, the MCF-7 cells were infected with Plasmids expressing RFP or GFP using Fugene 6 (Promega) at an early passage and were selected using 2 μg/ml puromycin (Sigma). During this experiment MCF7-GFP cells were kept always sensitive and MCF7-RFP resistant to Doxorubicin. To make the resistant cells we grew the MCF7-RFP in 0.1 mM Doxorubicin for three months. MCF7-RFP-DOX cells keep their resistant phenotype after freeze thaw or for several passages in regular media (not shown).

S1.2 3D spheroid co-culture

Perfecta3® 96-well Hanging Drop Plates and non-adhesive U-Shape Bottom 96-well plates were used to grow the primary spheres containing 20,000 cells total. Two experiments were conducted: 1) MCF7-GFP and MCF7-RFP-DOX cells were grown in mono-culture in high glucose conditions (10mM), and 2) both cells lines were grown in mono-culture in low glucose conditions (1mM). In each case the experiment had a starting density of 20,000 cells and physiological (7.4) pH. Each experiment had three replicates. An Incucyte microscope placed in 37 degree and 5% CO_2 was used to image the spheroid growth every 24h over 14 days.

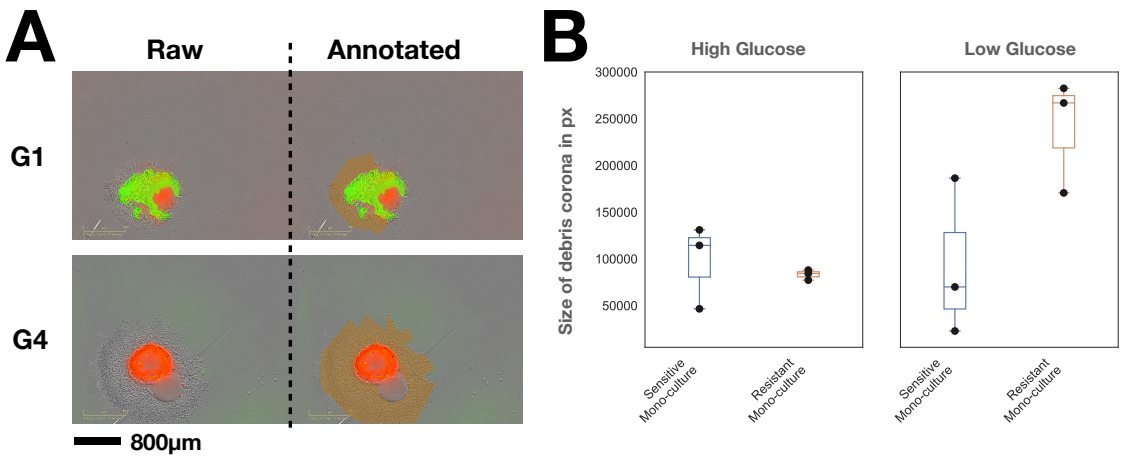

Figure S1: *Doxorubicin-resistant MCF7 cells (MCF7-RFP-DOX) show increased sensitivity to glucose starvation at 14d compared to their drug-sensitive counterpart (MCF7-GFP). A) Microscopy images with overlaid fluorescence illustrating the segmented debris corona for two wells (G1: sensitive mono-culture in low glucose conditions; G4: resistant mono-culture in low glucose conditions). In addition, this exemplifies the background noise (red signal in G1, green signal in G4) which has been removed from the data in Figure 1G. B) Comparison of the size of the debris corona between sensitive and resistant spheroids. While there is no difference in high glucose conditions (two-sample t-test:* $t_{3,3} = 0.54$, $p_{S>R} = 0.3$*), the difference is significant in low glucose conditions (two-sample t-test:* $t_{3,3} = 2.45$, $p_{S>R} = 0.035$*).*

S1.3 Image Analysis

Images and fluorescent intensity were extracted using in the Incucyte built-in software. Relative fluorescent units (RFUs) were normalized at each time point by averaging red/green fluorescence when the corresponding cell type was absent then subtracting this value from other fluorescent values of that cell type. To assess relative growth over time, RFUs were normalized relative to the fluorescence recorded 6h after seeding of the spheroids (6h so to allow for some settling-in time of the culture). All analysis and post-processing were carried out in Python 3.6.

S1.4 Analysis of Cell Turnover

In order to quantify the build-up of debris around the spheroids over time we manually segmented the corona around each spheroid at the final time point. The size of the corona in pixel is shown in Figure S1. As can be seen, the corona is noticeably larger around MCF7-RFP-DOX spheroids than around MCF7-GFP spheroids in low glucose conditions (Figure S1A).

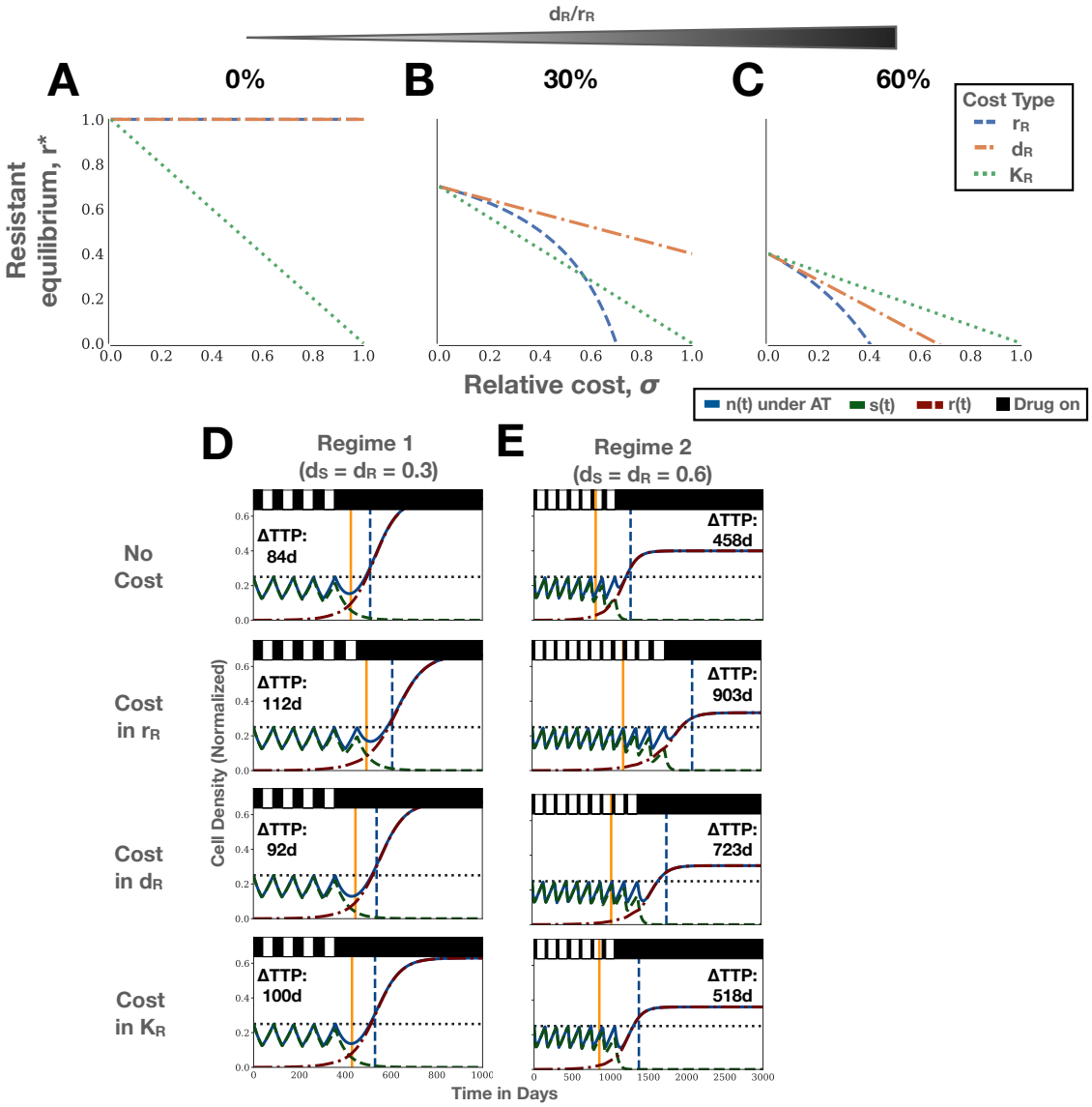

Figure S2: *Comparison of the impact of different manifestations of resistance costs. A-C) Plots of the resistant population equilibrium under costs in r_R ($r_r^*(c)$), d_R ($r_d^*(c)$), and K_R ($r_K^*(c)$), respectively. The smaller the value of r^*, the longer the achievable tumor control. Note that when $r^* \leq 0$ the resistant population will always go extinct. A) When there is no turnover, only a cost in K_R has an impact on r^*. B) For values of $d_R/r_R < 0.5$, there are two possible cases. For $c \leq 1 - \frac{1}{r_R/d_R - 1}$, a cost in K_R has the greatest impact. Otherwise a cost in r_R has a greater impact. C) For $d_R/r_R > 0.5$, a cost in r_R always has the greatest impact, followed by costs in d_R and K_R. D & E) Treatment dynamics under AT for Tumor 1 from Figure 3 ($(n_0, f_R) = (25\%, 0.1\%)$) without a cost and with a 10% cost in each of r_R, d_R and K_R, for two values of the replacement rate. D) Simulations corresponding to the parameters in B, in which a cost in K_R has the greatest effect on K_{Eff}. Interestingly, we see that here, due to the small value of n_0, a cost in r_R has the biggest impact on TTP. E) Simulations corresponding to C. Here, the results match those expected from Theorem S2.1, with again a cost in r_R being the most impactful. This illustrates that the comparison of different types of costs also depends on the density of sensitive cells in the tumor.*

S2 Extension to other types of cost

Throughout the main body of our manuscript we assume that the resistance cost manifests itself in the proliferation rate of the cells. However, it is plausible that it might manifests itself in the carrying capacity or the death rate (see, for example, Figure S1). To study the dynamics of such manifestations of a cost we will extend our model to the following more general form:

$$\frac{dS}{dt} = r_S \left(1 - \frac{S+R}{K_S}\right)(1 - d_D D(t))\, S - d_S S, \tag{1}$$

$$\frac{dR}{dt} = r_R \left(1 - \frac{R+S}{K_R}\right) R - d_R R, \tag{2}$$

$$N(t) = S(t) + R(t), \tag{3}$$

In the main manuscript we show that a key factor in adaptive therapy is the proximity of the tumor to the resistant population's "effective carrying capacity". That is its steady state level taking into account both environmental constraints (K) as well as the balance between birth and death rate. Thus, we will initially compare how d_R and K_R affect this equilibrium. Subsequently, we will show a set of simulations which demonstrates that when comparing different types of costs, we also need to take into account how each parameter affects the (density-independent) growth rate.

S2.1 Impact on the effective carrying capacity

The effective carrying capacity of the resistant population in this more general model is given by:

$$K_{\text{Eff}} = \left(1 - \frac{d_R}{r_R}\right) K_R \tag{4}$$

Equation (4) shows that costs in d_R and K_R also decrease the resistant population's effective carrying capacity, K_{Eff}, which will increase the benefit of AT, similar to what we have discussed for r_R. To compare the relative impact caused by each of the three types of cost, we define $R_r^* = \left(1 - \frac{d_R}{(1-c)r_R}\right) K_R$, $R_d^* = \left(1 - \frac{(1+c)d_R}{r_R}\right) K_R$, and $R_K^* = \left(1 - \frac{d_R}{r_R}\right)(1-c)K_R$ to be the population equilibria under a relative cost of c (> 0) in r_R, d_R, and K_R, respectively. In Figure S2A-C we plot the three functions for three different values of the cell replacement rate d_R/r_R. When $d_R/r_R = 0$, only a cost in K_R has an impact on the the effective carrying capacity (Figure S2A). When we increase d_R/r_R to 30%, small costs will have the greatest impact if they are in K_R, but if the costs are larger, they will have more impact in r_R (Figure S2B). The transition occurs when the $R_r^*(c)$ and $R_K^*(c)$ lines intersect at $\frac{d_R}{r_R} = \frac{1-c}{2-c}$ (Figure S2B). As we will show below, this behavior holds true for $0 < \frac{d_R}{r_R} < 0.5$. Finally, when $\frac{d_R}{r_R} > 0.5$, a cost in r_R will have the greatest impact, followed by costs in d_R, and K_R, respectively.

We formally prove these observations in the following theorem:

Theorem S2.1. *Let* $R_r^* = \left(1 - \frac{d_R}{(1-c)r_R}\right) K_R$, $R_d^* = \left(1 - \frac{(1+c)d_R}{r_R}\right) K_R$, *and* $R_K^* = \left(1 - \frac{d_R}{r_R}\right)(1-c)K_R$ *denote the population equilibria under a relative cost of* c (> 0) *in* r_R, d_R, *and* K_R, *respectively. Then:*

1. *The impact of a cost in* r_R *will always be greater than the impact of a cost in* d_R. *That is,* $R_r^* > R_d^*, \forall c \in (0,1)$.

2. *Provided* $d_R < \frac{c}{1+c} r_R$, *the impact of a cost in* K *will be greater than the impact of a cost in* d_R $(R_K^* > R_r^*)$. *Otherwise a cost in* d_R *will have a greater impact.*

3. *The impact of a cost in* K *will be greater than the impact of a cost in* r_R $(R_K^* > R_r^*)$ *provided* $d_R > \frac{1-c}{2-c} r_R$. *Otherwise a cost in* r_R *will have a greater impact.*

Proof. Claim 1: Comparing R_r^* and R_d^* we find:

$$\begin{aligned}
&R_r^* > R_d^* \\
\Leftrightarrow &\left(1 - \frac{d_R}{(1-c)r_R}\right) K_R > \left(1 - \frac{(1+c)d_R}{r_R}\right) K_R \\
\Leftrightarrow &(1+c) < \frac{1}{1-c} \\
\Leftrightarrow &c^2 > 0,
\end{aligned}$$

so that $R_r^* > R_d^*, \forall c \in (0,1)$.

Claim 2: Similarly, comparing R_K^* and R_d^* gives:

$$\begin{aligned}
&R_K^* > R_d^* \\
\Leftrightarrow &\left(1 - \frac{d_R}{r_R}\right)(1-c)K_R > \left(1 - \frac{(1+c)d_R}{r_R}\right) K_R \\
\Leftrightarrow &-c(1+c)d_R - r_R(1+c) + c\, r_R(1+c) > -r_R \\
\Leftrightarrow &d_R < \frac{c}{1+c} r_R,
\end{aligned}$$

where we have skipped some steps for brevity.

Claim 3: Finally, comparing R_K^* and R_r^* yields:

$$\begin{aligned}
&R_K^* > R_r^* \\
\Leftrightarrow &\left(1 - \frac{d_R}{r_R}\right)(1-c)K_R > \left(1 - \frac{d_R}{(1-c)r_R}\right) K_R \\
\Leftrightarrow &-(1-c^2)\frac{d_R}{r_R} - c(1-c) > -\frac{d_R}{r_R} \\
\Leftrightarrow &d_R > \frac{1-c}{2-c} r_R,
\end{aligned}$$

where we again have skipped some steps for brevity. □

There are two important conclusions to draw from this analysis. Firstly, a cost in the growth rate will always have a greater impact than the same relative increase in the death rate (unless $d_R = 0$). Secondly, the relative importance of each of the three parameters depends on the ratio d_R/r_R.

S2.2 Comparison of the AT treatment dynamics under different types of cost

How do the different possible manifestation of a cost affect treatment dynamics? In Figures S2C & D, we show the AT treatment dynamics for a 10% cost in each of r_R, d_R and K_R for Tumor 1. Firstly, we consider the regime $d_R/r_R < 0.5$ in which a cost in K_R will have the greatest impact on K_{Eff}. Interestingly, we find that - contrary to our expectations from Theorem S2.1 - a cost in r_R has the largest impact on TTP (Figure S2D). As we can see from Figure S2D, the resistant population takes longer to expand and more AT cycles can be completed when there is a cost in r_R compared to when there is a cost in K_R (4 vs 5 cycles). To explain this, we rewrite Equation (2) as:

$$\frac{1}{r_R}\frac{dR}{Rdt} = \underbrace{\left(1 - \frac{d_R}{r_R}\right)}_{\substack{\text{Density-Independent} \\ \text{Expansion}}} - \underbrace{\frac{S}{K_R}}_{\substack{\text{Density-Dependent} \\ \text{Inhibition}}} \tag{5}$$

where we again are assuming that intra-specific competition can be neglected until close to progression ($R << S$). We see that the benefit from the reduced carrying capacity depends on the density of sensitive cells. Is the tumor far from carrying capacity, as is the case here ($S \leq 0.25$), the benefit is small as the competition isn't very strong. In contrast, costs in r_R (and d_R) have an impact *independent* of the proximity to carrying capacity.

In the second case, we assume that the replacement rate is greater than 0.5. While it is probably not biologically realistic, we include this case for completeness. We find that here the order in which cost extends TTP coincides with what would be expected from Theorem S2.1 (Figure S2E). This is because the costs in r_R and d_R reduce both the density dependent, and the independent-growth rate more than the cost in K_R (Figure S2E).

This analysis demonstrates again that in order to understand the impact of a resistance cost we have to consider not only the cost itself, but also the context in which it occurs (here replacement rate and initial proximity to carrying capacity). Furthermore it shows that the two ways we discuss for improving AT (decreasing K_R or increasing d_R/r_R) will amplify resistance costs regardless of their type.

S3 Non-Dimensionalization & Numerical Methods

S3.1 Non-Dimensionalization

In order to reduce the number of free variables, we non-dimensionalize Equations (1) - (3). Given that we are interested in studying the treatment dynamics if we change the characteristics of the resistant cells relative to the sensitive cells, we base our scales on the sensitive population. Specifically, we will use the following transformations:

$$\tau = r_S t, \quad s = \frac{S}{K}, \quad r = \frac{R}{K}, \quad c = \frac{D}{D_{\text{Max}}}, \quad \text{and} \quad n = \frac{N}{K}.$$

This yields:

$$\frac{ds}{d\tau} = (1 - s - r)\,(1 - \hat{d}_D\, c(\tau))\, s - \hat{d}_T s, \tag{6}$$

$$\frac{dr}{d\tau} = \hat{r}_R\,(1 - s - r)\, r - \hat{d}_T r, \tag{7}$$

$$n(\tau) = s(\tau) + r(\tau), \tag{8}$$

where:

$$\hat{d}_D = 2d_D, \quad \hat{d}_T = \frac{d_T}{r_S}, \quad \text{and} \quad \hat{r}_R = \frac{r_R}{r_S}.$$

The initial conditions transform to:

$$n(0) = \frac{N_0}{K} := n_0, \quad s(0) = \frac{S_0}{K} := s_0, \quad \text{and} \quad r(0) = \frac{R_0}{K} := r_0,$$

and the treatment schedules are adjusted accordingly as well (not shown). Finally, for notational convenience we will define $f_S := S_0/N_0$ and $f_R := R_0/N_0$ as the initial fractions of sensitive and resistant cells, respectively.

S3.2 Numerical Methods

The equations were solved using the RK5(4) explicit Runge-Kutta scheme [1] provided in Scipy (specifically, the SCIPY.INTEGRATE.ODE class). Adaptive therapy was implemented by simulating an interval $[t, t + \Delta t]$ at a time, and subsequently updating the dose for the next interval according to the algorithm in Equation 4. In preliminary experiments we tested different values of Δt and found $\Delta t = 1$d to provide a good trade-off between speed and accuracy (not shown). All simulations were carried out in Python 3.6, using Scipy 1.1.0 and Numpy 1.15.1. Visualizations were produced with Pandas 0.23.4, Matplotlib 2.2.3, and Seaborn 0.9.0. The code is available at `https://github.com/MathOnco/AT_costOfResistance_LVModel`.

S4 Steady State Analysis

For completeness we here analyze the more general model discussed in Section S2 of which the model which forms the focus of the main paper is a special case. Also, so to explicitly show the relationship of the steady states with the system parameters we will here work with the dimensional form of the equations. We will begin with a general discussion before providing two specific examples illustrating the key features of the phase plane dynamics which are driving our results. Assuming continuous therapy at dose $D(t) = D^*$ Equations (1)-(2) have the following steady states:

- Tumor Elimination (SS1): $(S^*, R^*) = (0, 0)$. A linear stability analysis gives eigenvalues $\lambda_1 = r_S(1 - d_D D^*) - d_S$ and $\lambda_2 = r_R - d_R > 0$, which shows that this state is always unstable and so, unless there are no resistant cells in the tumor or $d_R > r_R$, tumor elimination is not possible in this model. This is because there is no mechanism in this model to prevent the outgrowth of resistant cells except for inhibition from sensitive cells.
- A Fully Sensitive Tumor (SS2): $(S^*, R^*) = \left(\left(1 - \frac{d_S}{r_S(1-d_D D^*)}\right) K_S,\, 0\right)$ which corresponds to a tumor consisting entirely of sensitive cells. This state has eigenvalues $\lambda_1 = r_R - d_R - r_R\left(1 - \frac{d_S}{r_S(1-d_D D^*)}\right)\frac{K_S}{K_R}$ and $\lambda_2 = r_S(d_D D^* - 1)\left(1 - \frac{d_S}{r_S(1-d_D D^*)}\right)$, so that its feasibility and stability depend on the effective drug kill rate $d_D D^*$, and the ability of the resistant cells to invade the equilibrium, which is determined by the balance of terms expressed in λ_1.
- A Fully Resistant Tumor (SS3): $(S^*, R^*) = \left(0,\, \left(1 - \frac{d_R}{r_R}\right) K_R\right)$ which describes a tumor consisting entirely of drug resistant cells. This state has eigenvalues $\lambda_1 = r_S(1-d_D D^*)\left(1 + \left(\frac{d_R}{r_R} - 1\right)\frac{K_R}{K_S}\right) - d_S$ and $\lambda_2 = d_R - r_R < 0$, which implies its stability is dependent on the sign of λ_1.
- Coexistence (SS4): $(S^*, R^*) = \left(S,\, \left(1 - \frac{d_R}{r_R}\right) K_R - S\right)$, which describes a set of tumors consisting of a mixture of sensitive and resistant cells. This set only exists if the two non-zero nullclines precisely overlap (see Figure S3A for an illustration). No simple analytical form is available for the corresponding eigenvalues, and thus, they will be omitted here.

Having discussed the eigenvalues in general we will briefly show four specific examples to illustrate the impact of the turnover and a cost of resistance on the phase plane dynamics. To do so, we will again adopt the simplifying assumptions that $d_S = d_R := d_T$ and $K_S = K_R := K$. Unless otherwise stated simulations were done with the parameters from Table 1.

S4.1 No turnover

Assuming $d_T = 0$, we obtain the eigenvalues shown in Table S1. We note that r_R has no effect on the position of the steady states and merely scales the eigenvalues so that a cost of resistance will have no influence on the structure of the phase space in this case. Thus, to simplify the following analysis we will assume there is no cost ($r_R = r_S$).

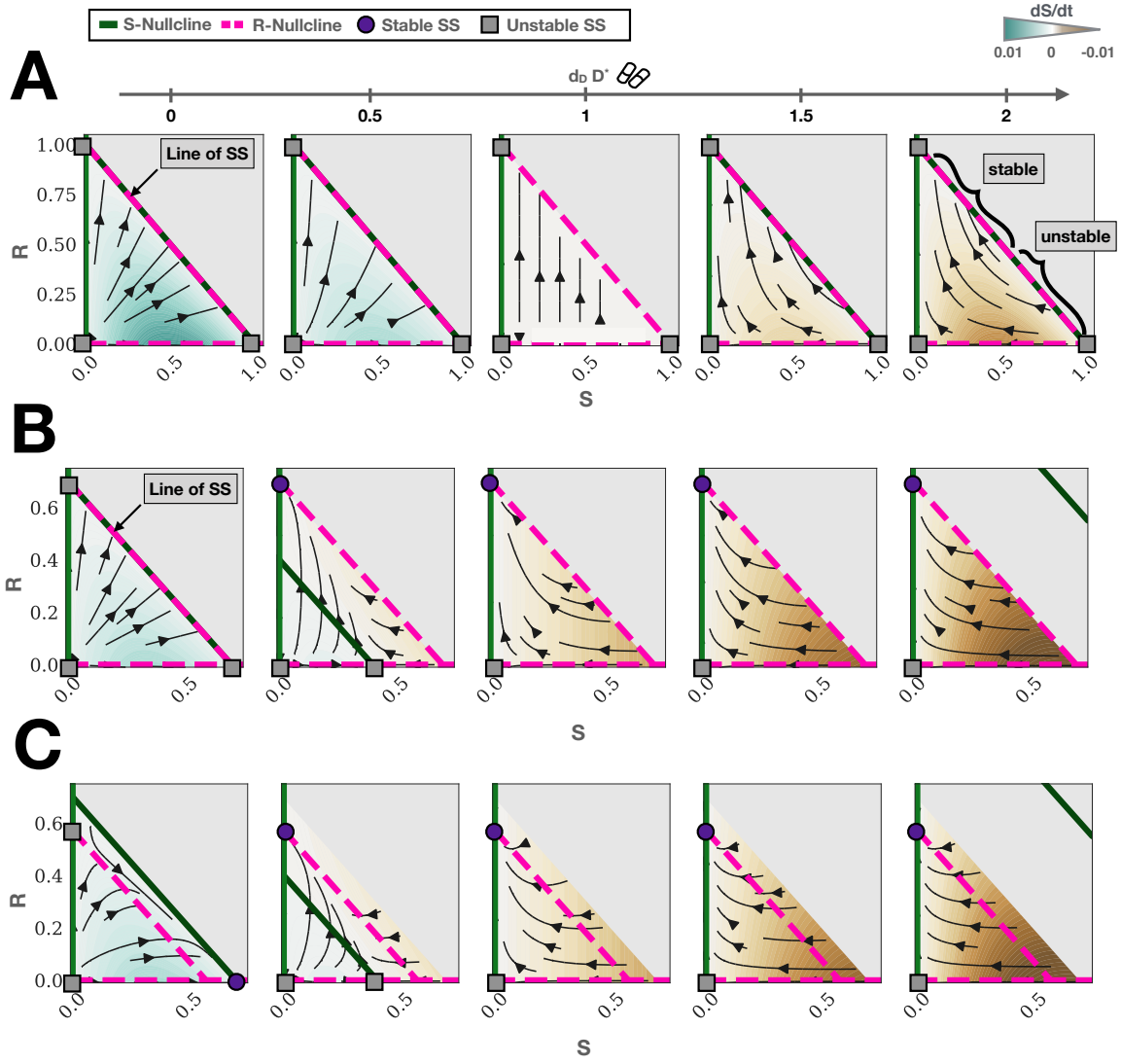

Figure S3: *Phase planes of the model (Equations* (6) *and* (7)*) under continuous therapy with increasing levels of drug kill, $d_D D^*$ (parameters as in Table 1). We assume no cost of resistance ($r_R = r_S$). SS stands for steady state. Grey area corresponds to tumors which are excluded from the analysis because they would shrink even without treatment. A) No turnover and no cost ($d_T = 0$, $r_R = r_S$). There is a continuum of steady states (SS4) given by $S + R = 1$. For $d_D D^* < 1$ the tumor continues to grow until it reaches carrying capacity on SS4. For $d_D D^* > 1$ sections of SS4 become unstable and we see the formation of heteroclinic orbits between unstable and the stable section of SS4. This represents tumors which are largely sensitive so that they will initially experience tumor shrinkage, but will subsequently recur due to the outgrowth of resistance. B) Turnover but no cost ($d_T = 0.1$, $r_R = r_S$). Unless $d_D D^* = 0$, the tumor becomes fully resistant over time. C) Turnover and cost ($d_T = 0.3$, $r_R = 0.7$). Provided the tumor is treated at low dose ($d_D D^* < 1 - r_R/r_S$), it can be maintained fully sensitive and decreased in size (not shown). If the dose is escalated beyond this threshold, the tumor will evolve to become fully resistant.*

State	Description	A) No Turnover ($d_T = 0$)	B) With Turnover ($0 < d_T < r_S, r_R$)
SS1	*Tumor Elimination*	$\lambda_1 = \mathbf{r_S}(\mathbf{1} - \mathbf{d_D D^*})$ $\lambda_2 = r_R$	$\lambda_1 = \mathbf{r_S}(\mathbf{1} - \mathbf{d_D D^*}) - \mathbf{d_T}$ $\lambda_2 = r_R - d_T$
SS2	*Sensitive Tumor*	$\lambda_1 = 0$ $\lambda_2 = \mathbf{r_S}(\mathbf{d_D D^* - 1})$	$\lambda_1 = \mathbf{d_T}\left(\frac{\mathbf{r_R}}{\mathbf{r_S}(\mathbf{1-d_D D^*})} - \mathbf{1}\right)$ $\lambda_2 = \mathbf{r_S}(\mathbf{d_D D^* - 1})\left(\mathbf{1} - \frac{\mathbf{d_T}}{\mathbf{r_S}(\mathbf{1-d_D D^*})}\right)$
SS3	*Resistant Tumor*	$\lambda_1 = 0$ $\lambda_2 = -\mathbf{r_R}$	$\lambda_1 = \mathbf{d_T}\left(\frac{\mathbf{r_S}}{\mathbf{r_R}}(\mathbf{1} - \mathbf{d_D D^*}) - \mathbf{1}\right)$ $\lambda_2 = \mathbf{d_T} - \mathbf{r_R}$
SS4	*Coexistence*	No simple form available	No simple form available

Table S1: *Eigenvalues for the cases considered in Figure S3 (assuming $d_D D^* \neq 1$). **Bolded values** indicate eigenvalues which are negative in at least part of the parameter space.*

Both SS2 and SS3 have zero eigenvalues because they lie on the manifold of steady states given by SS4. By considering the phase flow of Equations (6) & (7) one can see that between $d_D D^* = 0$ and $d_D D^* = 1$, the tumor will keep growing and converge to a point on SS4 (Figure S3A). The greater the value of $d_D D^*$, the larger the proportion of resistant cells at equilibrium. When $d_D D^* = 1$, dS/dt becomes exactly 0 everywhere (Figure S3A; see also Equation 1). As $d_D D^*$ is increased above 1, the sign of dS/dt switches (Figure S3A). Moreover, parts of the line SS4 become unstable, and we observe the formation of heteroclinic orbits connecting the unstable portions of SS4 to the stable portions of SS4 (Figure S3A). Biologically, the transition through $d_D D^* = 1$ represents a transition from when the drug only reduces the net growth of the population to when it actually causes decreases in the population size. The heteroclinic orbits represent tumors which initially shrink in size but subsequently recur. Interestingly, the fully resistant state becomes the globally absorbing state only as $d_D D^* \to \infty$. This is because the resistant cells protect the sensitive cell by saturating the environment, thereby preventing them to divide which makes them no longer sensitive to the drug.

S4.2 With turnover

If we assume that turnover is present ($0 < d_T < r_S, r_R$) we obtain the eigenvalues given in the right-hand side column of Table 1. To begin with, let us assume that there is no cost of resistance ($r_R = r_S$). If $d_D D^* = 0$, then we again have a line of steady states, but this time the tumor saturates below the carrying capacity, K (Figure S3B). Importantly, if the drug kill is increased, then the S-nullcline given in dimensional form by $S(t) = \left(1 - \frac{d_T}{(1-d_D D^*) r_S}\right) K - R$, is now translated

downwards. As a result, for $0 < d_D D^* < 1$, SS4 disappears and SS3 becomes stable ($\lambda_1, \lambda_2 < 0$) whereas SS2 is unstable ($\lambda_1 > 0$; see also Figure S3B). Thus, in contrast to when turnover is absent, in the presence of turnover the tumor evolves to become fully resistant even if treated at a very low dose (Figure S3B). When $d_D D^*$ is increased above 1, SS2 takes on a value above K which converges to K from above as $d_D D^* \to \infty$ (see the expression for SS2 in Section S4 and Figure S3B). Whilst positive, this state is not biologically realistic as it implies that the population can grow beyond the environmental carrying capacity.

Finally, we consider the impact of a cost of resistance in this setting ($r_R < r_S$). From Table S1 we can see that provided $d_D D^* < 1 - r_S/r_R$, SS2 is stable whereas SS3 is unstable. Thus, in the presence of a cost low dose treatment can shrink the tumor whilst maintaining it stably sensitive (Figure S3C). However, if the drug kill is intensified beyond $1 - r_S/r_R$ SS2 becomes unstable and SS3 becomes stable (Table S1) and the tumor will become fully resistant over time (Figure S3C).

S5 Density-Dependent Death Model

The expansion of cell populations in human tissues is controlled by inter-cellular signaling and competition for space and resources. Most commonly, this regulation is modeled to take place via the birth rate, so that cells proliferate less often in a more crowded environment, due to, for example, contact inhibition or spatial occlusion whilst the cell death rate remains constant (Figure S4A). This gives rise to a tissue in which the per-capita proliferation rate decreases until it matches the death rate at carrying capacity. In contrast, one may also assume that density regulation occurs via the death rate. In such a model cells proliferate at a constant rate and the death rate increases due to crowding (Figure S5A). This results in a tissue in which cell production is at its largest at carrying capacity and replacement is much more rapid than in the density-dependent birth model. In the human body most likely both proliferation and death rate are density-dependent, in a fashion which depends on the tissue type. Following previous studies we have used a density-dependent birth model in the main text of this manuscript. To show that our results hold true also in a density-dependent death model, in fact that they are amplified in such a model, we here consider a density-dependent death version of our model.

S5.1 The model

We re-formulate our model (Equations (1) - (3)) so that the density dependence is in the death rate. This yields the following equations:

$$\frac{dS}{dt} = r_S \left(1 - \frac{2d_D}{D_{Max}} D(t)\right) S - d_T^{\dagger} \left(\frac{S+R}{K}\right) S, \tag{9}$$

$$\frac{dR}{dt} = r_R R - d_T^{\dagger} \left(\frac{S+R}{K}\right) R, \tag{10}$$

$$N(t) = S(t) + R(t), \tag{11}$$

All parameters but the death rate $d_T^{\dagger}$ and the carrying capacity K maintain the same meaning and value as in the original model (Table 1). This is because in the density-dependent birth model the death rate d_T describes the average rate of cell death (Figure S4A). In contrast, in the density-dependent death model $d_T^{\dagger}$ captures death rate observed when the population reaches the level K. Assuming K describes a maximum allowable homeostatic cell density, then $d_T^{\dagger}$ would be the death rate observed at this density (Figure S4A). Note that unlike in the density-dependent birth model, K is not a hard boundary here, and if the growth rate is increased it is possible for the population to exceed K.

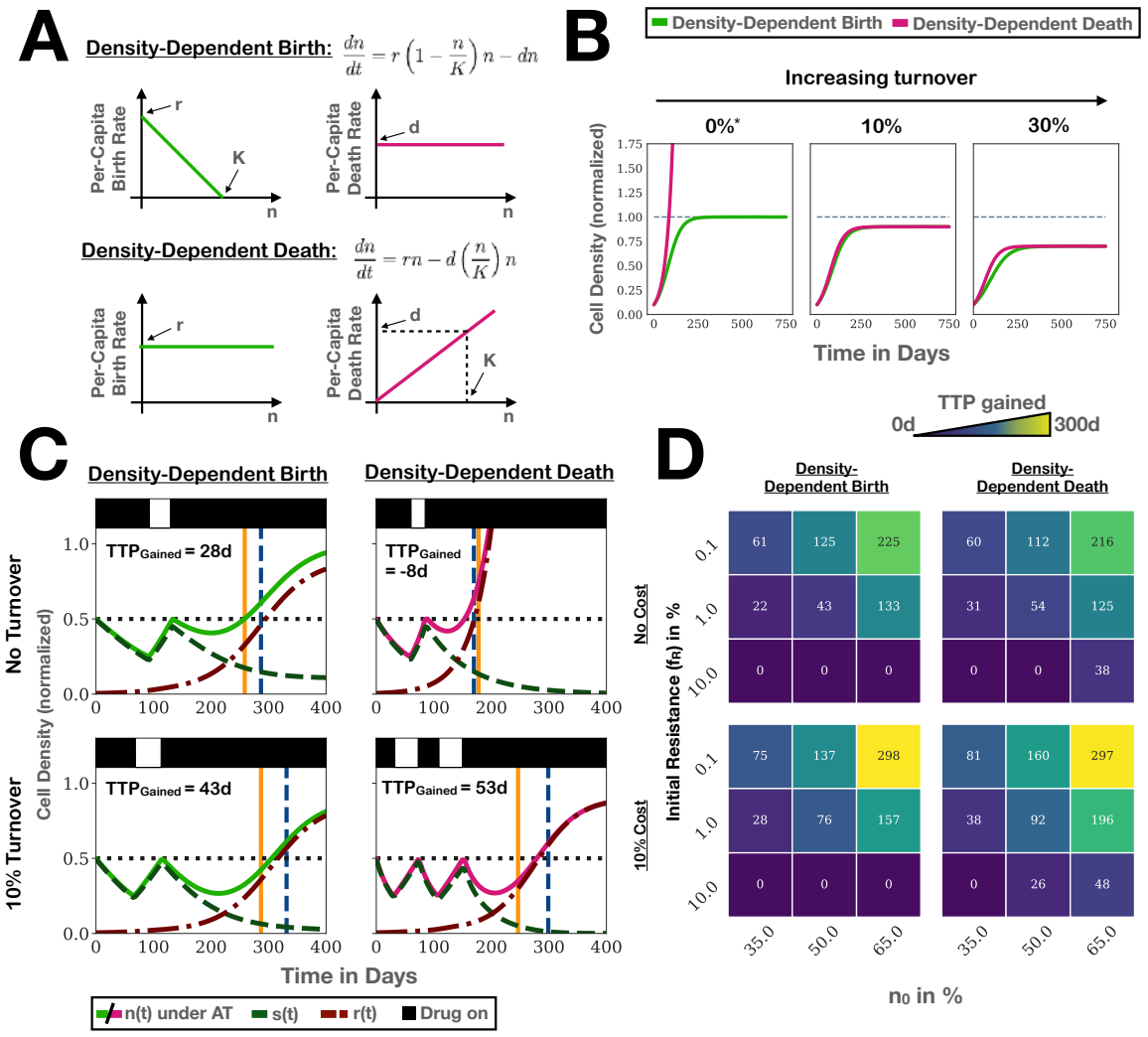

Figure S4: *Validation of our results in a model in which crowding affects not the birth but the death rate. A) Example of a simple density-dependent birth, and death model, respectively. In the former, the per-capita birth rate decreases with population density, while the per-capita death rate remains constant. In the latter, per-capita death increases whilst birth remains constant. B) Growth of a single population according to a density-dependent birth or death model for different turnover rates (equations are those from A) which are equivalent to Equations* (9)-(11) *with one population set to 0; $n_0 = 10\%$). The turnover rates shown are those in the density-dependent birth model. For the density-dependent death model these were transformed using Equation* (12)*, so that both models produce the same population density at carrying capacity. The only exception is $d_T = 0$, for which also $d_T^\dagger = d_T = 0$. C) Representative simulations comparing adaptive and continuous therapy for the density-dependent birth and the death model ($(n_0, f_R) = (50\%, 1\%)$; $\hat{r}_R = 100\%$). In the absence of turnover there is no benefit for adaptive therapy in the density-dependent death model as the growth of sensitive and resistant cells is decoupled. In the presence of turnover, there is a benefit of adaptive therapy in both models and this is greater in the density-dependent death model. D) TTP gained by adaptive therapy according to the density-dependent birth model and the density-dependent death model ($d_T = 10\%$, $d_T^\dagger$ determined by Equation* (12)*). The density-dependent death model predicts a greater and more wide-spread benefit of adaptive therapy in most cases, which is further amplified if a cost is present. This corroborates our hypothesis that turnover may be an important factor in adaptive therapy.*

S5.2 Results

S5.2.1 No turnover

To begin with we consider the case of no turnover, and set both $d_T^\dagger$ and d_T to 0. As a result, the two models make very different predictions. Focussing just on a single population, we see that the density-dependent birth model predicts that the population will saturate at carrying capacity (Figure S4B). In contrast, the density-dependent death model predicts exponential growth as by removing d we have removed all density-dependence (Figure S4B).

In Figure S4C we show how this translates to treatment response. In the absence of turnover ($d_T^\dagger = d_T = 0$), both models predict failure after a single cycle, with the density-dependent death model failing before the birth model. Importantly, while the density-dependent birth model predicts a benefit for adaptive therapy, this relationship is inverted in the density-dependent death model. This is because setting $d_T^\dagger = 0$ has decoupled sensitive and resistant cells, so that the resistant cells now simply grow exponentially. Withholding treatment in this situation simply increases the tumor burden with no benefit for controlling resistance. This is true even if a cost is added (not shown), and is further evidence that in simple models such as ours, adaptive therapy is predicted only to provide a minimal disadvantage in survival, even if it fails (see also [2] for a more detailed discussion of this observation).

S5.2.2 With turnover

In order to allow comparison of the two models we will use the following transformation which maps the death rates so that both models produce the same untreated steady state:

$$d_T^\dagger = \frac{1}{1 - d_T/r_S}, \tag{12}$$

To illustrate this, in Figure S4B we compare the two models in absence of treatment for a single population. As intended, the two models converge to the same steady state. However, the density-dependent death model converges more rapidly due to its relatively higher per-capita growth rate (Figure S4B).

Next we examine the tumor's response to treatment. We find that both models now predict a benefit for adaptive therapy (S4C). Moreover, the benefit is larger in the density-dependent death model than in its density-dependent birth counterpart. Performing a parameter sweep over different values of n_0 and f_R corroborates this observation in most cases (Figure S4D). Adding a cost in this context increases TTP for both model, where again we see generally larger increases in the density-dependent death than in the birth model (Figure S4D). In addition, while there is no benefit for adaptive therapy for a resistance fraction of 10% in the density-dependent birth model, there is a benefit in the death model, especially when a cost is present (Figure S4D).

S5.3 Conclusion

Overall, the density-dependent death model qualitatively re-capitulates the results from the main manuscript: Adaptive therapy can provide benefits even without a resistance cost, and is facilitated by a higher turnover rate. In fact, the predicted gains are generally larger than in the density-dependent birth model. This further supports our hypothesis that the rate and nature of tissue turnover may be an important factor in adaptive therapy. However, there are also differences in the timing of progression and the lengths of on- and off-phases during adaptive therapy between the two models. It would be interesting to study this in more detail in the future, as it suggests that the growth kinetics in the target tissue (density-dependent birth vs death) might need to be considered when developing tumor-specific strategies.

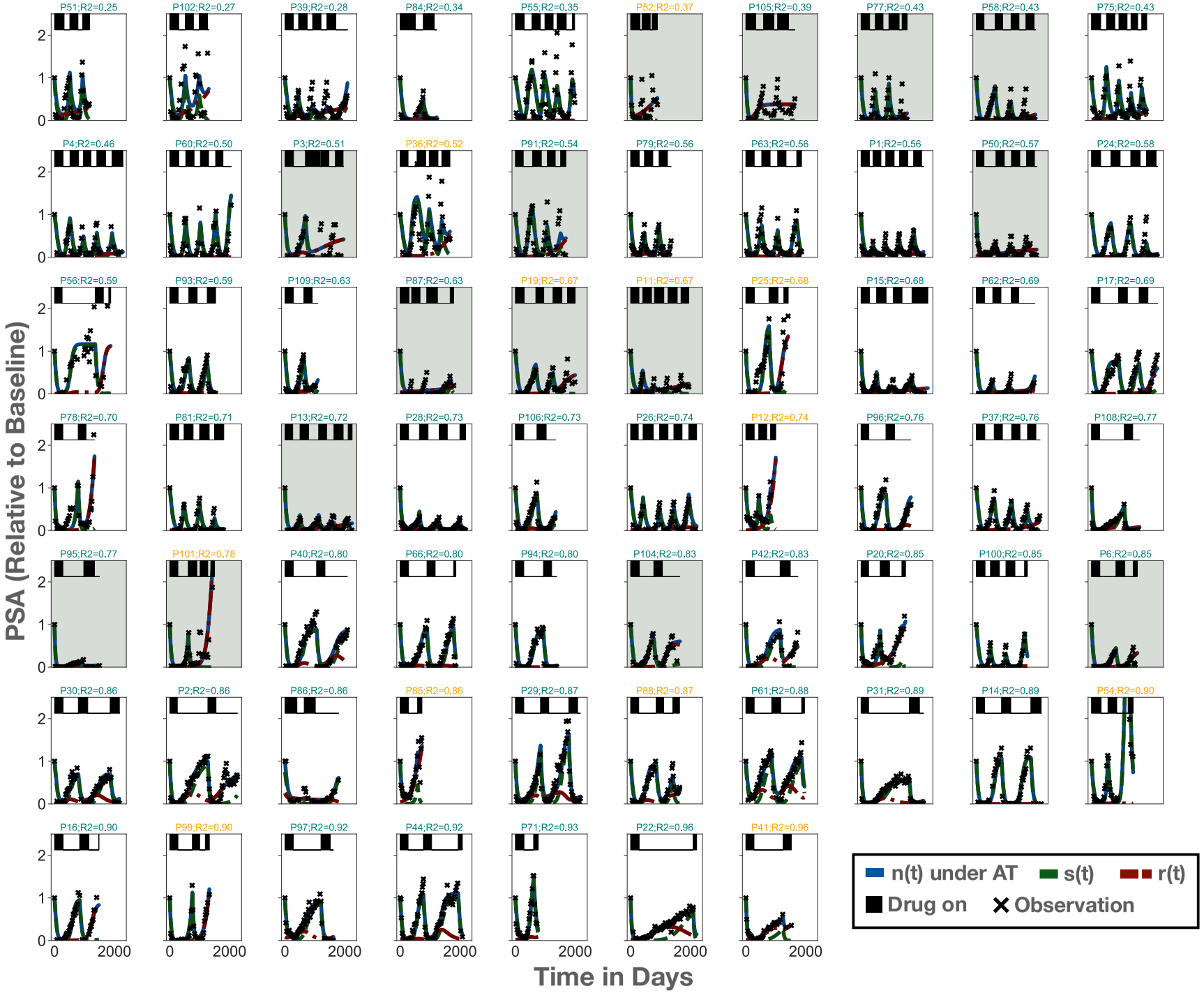

Figure S5: *Overview of all 67 patient fits arranged by the r^2 value of the best model fit. Title color indicates whether a patient relapses (orange) or not (green). Patients who were excluded from further analysis due to poor model fits are marked with a grey background.*

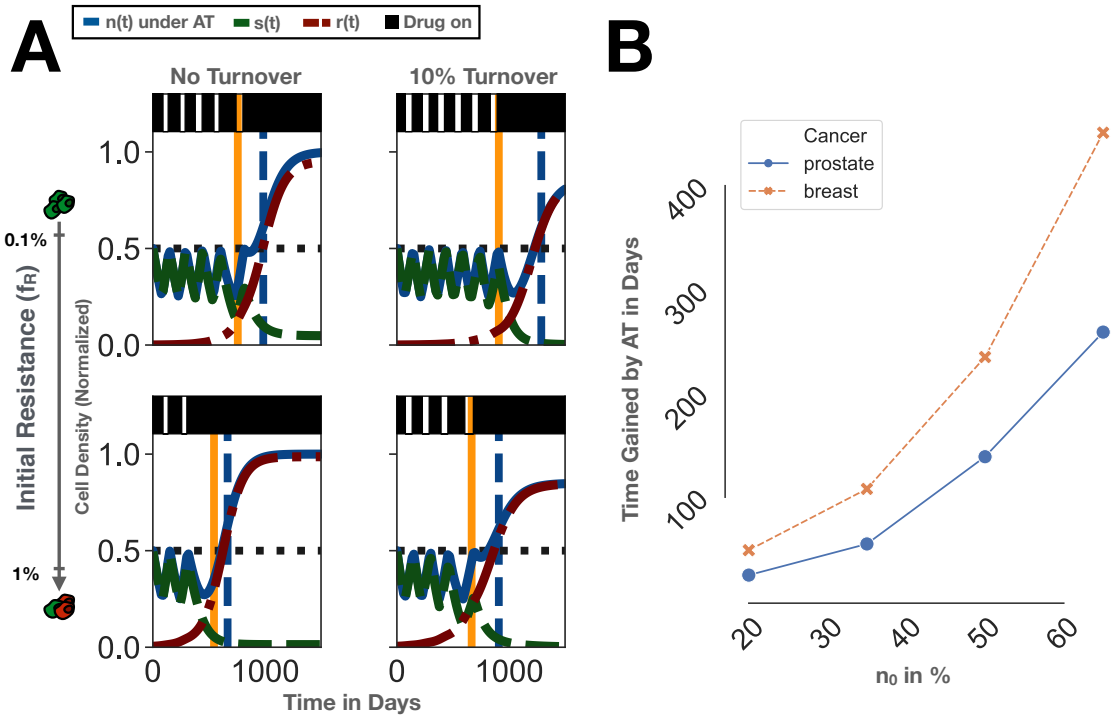

Figure S6: *Impact of cost and turnover for parameters modeling breast cancer treatment with doxorubicin. Parameters are adopted from the 2-d, in vitro cell culture experiments in Gallaher et al [3], and are as follows:* $r_S = 0.017d^{-1}$, $\hat{r}_R = 0.67$, $\hat{d}_D = 1.78$. *A) Simulations comparing adaptive and continuous treatment with and without turnover for two levels of initial resistance. In agreement with the results for prostate cancer in the main manuscript, the benefit of adaptive therapy increases for lower initial resistance fractions and higher turnover* ($n_0 = 50\%$). *B) Time gained by adaptive therapy as a function of the initial proximity to carrying capacity for a turnover rate of 10%, as reported by Lloyd et al [4]* ($f_R = 1\%$). *This shows that also in this setting adaptive therapy will be most effective if the tumor is close to carrying capacity. Moreover, to compare these results to those in the main manuscript we repeat the analysis for the prostate specific parameters in Table 1, assuming the same cost and turnover* ($\hat{r}_R = 0.67$, $\hat{d}_T = 0.1$). *This shows relatively good agreement, with the benefit in breast cancer being even slightly larger than those for prostate cancer. We stress, however, that the main aim of this paper was not to make disease specific predictions, but to understand the role of resistance costs in a general fashion. Our main results are the general principles we have uncovered, and it will be the subject of future research to test these in specific disease settings using dedicated mathematical and experimental models.*

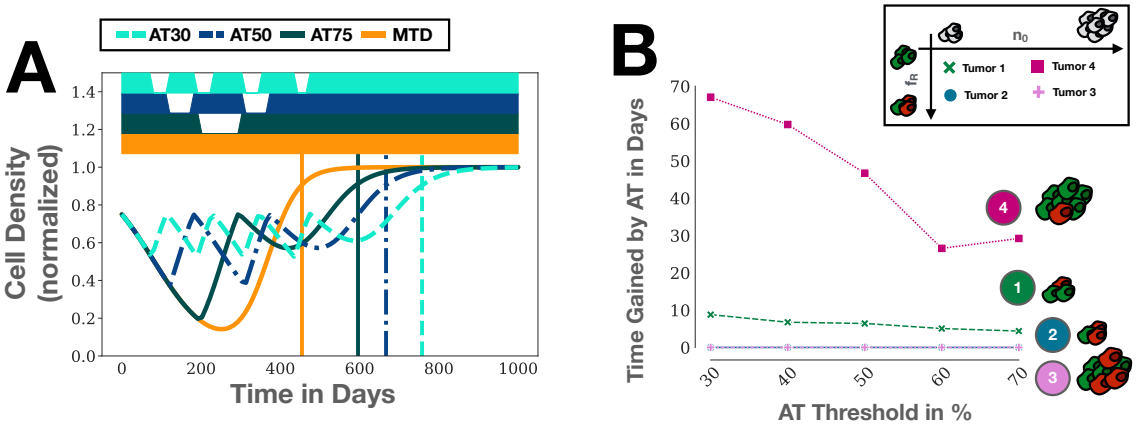

Figure S7: *Adaptive treatment algorithms which withdraw treatment early maximize TTP in this model. A) Comparison of continuous therapy with four adaptive treatment strategies which withdraw drug after a 30%, 50%, or 75% burden reduction, respectively. The protocol with the smallest burden reduction (30% - corresponding to partial response under the RECIST criteria) maximizes TTP. Parameters:* $(n_0, f_R) = (75\%, 0.1\%)$*;* $\hat{d}_T = 0$*;* $\hat{r}_R = 100\%$*. B) Time gained by adaptive therapy as a function of the drug withdrawal threshold for Tumors 1-4 from Figure 3a. This illustrates that the smallest threshold maximizes TTP across a range of conditions.*

S6 Justification of the choice of turnover rates

Pathological Type	T_V (in days) (95% CI)	T_{Pot} (in days)	Estimated Growth Fraction (in %)	Cell Loss Factor (in %)	Estimate for $\hat{d}_T$ (=GF×ϕ)
Embryonal tumours	27 (22-33)	1.66	90	94	84.4%
Hemato-sarcoma	29 (23-37)	1.7	90	94	84.4%
Mesenchymal Sarcomas	41 (35-50)	13.2	11	68	7.48%
Squamous cell carcinoma	58 (48-70)	6.0	25	90	22.5%
Adeno-carcinoma	83 (72-96)	23.8	6	71	4.3%

Table S2: *Proliferation rates and cell loss factors measured in human tumors (taken from the meta-analysis by Malaise and colleagues in [5]).*

While cell turnover due to apoptosis, necrosis and immune predation is recognized as a feature of many tumors, little is known about the rate at which tumor cells die. Most available data infer the amount of cell loss indirectly using a method introduced by Gordon Steel in the 1960s [6, 7, 8]. The idea is to estimate the theoretically possible ("potential") doubling time, T_{Pot}, achieved in the absence of any cell death, and the actually observed volumetric doubling time of a tumor, T_V. By comparing these values one can compute the "cell loss factor", ϕ, defined as $\phi = 1 - T_{Pot}/T_V$ which represents the relative rate of cell death to proliferation (assuming an exponentially growing tumor). The greater the value of ϕ, the greater the loss of cells due to cell death, predation, or emigration [6, 7, 8].

T_V is estimated from x-ray, CT or MRI images. T_{Pot} is obtained by measuring the fraction of cells in S-phase in the tumor via halogenated pyrimidine, bromo- or iododeoxyuridine labelling. Cells carrying out DNA synthesis incorporate these agents into their DNA, and can subsequently be identified using histological techniques or flow cytometry. The proportion of labelled cells is termed the labelling index (LI). To obtain T_{Pot}, the LI is adjusted to account for proliferating cells which are not currently in S-phase and is multiplied by an estimate of the cell cycle time, based on the time required for DNA synthesis (T_S). This gives $T_{Pot} = \lambda T_S/LI$, where λ denotes the proportion of the cell cycle spent in the S-phase. For a detailed review of the process of estimating T_{Pot} see [9].

In Table S2 we show estimates for the cell loss factor for a range of human tumors. These are all well in the excess of 50% - an observation which has been corroborated by a large number of

studies over the years (see [5, 7, 10] for extensive reviews). To translate estimates for ϕ to values of our model parameter $\hat{d}_T$ we need to note that ϕ compares the cell turnover rate to the effective proliferation rate of the population (which takes into account the actual fraction of proliferating cells), not the intrinsic growth rate. To illustrate this, consider a logistic model of a growing tumor. Let $N(t)$ denote the total number of cells and assume that cells divide and die at rates r_T and d_T, respectively, so that: $dN/dt = r_T(1 - N/K)N - d_T N$. If we were to measure this tumor at time t^* we would observe a growth fraction of $(1 - N(t^*)/K)$ and estimate (making the assumption of the Steel method that this growth fraction remains constant), that $T_{\text{Pot}} = \ln(2)/r_T(1 - N(t^*)/K)$. The actual volumetric doubling time (again assuming the growth fraction remains constant) would be $T_{\text{V}} = \ln(2)/(r_T(1 - N(t^*)/K) - d_T)$. Thus, $\phi = d_T/(r_T(1 - N(t^*)/K))$. To obtain $\hat{d}_T := d_T/r_T$, we therefore want to scale the observed values of ϕ by the fraction of dividing cells. Applying this calculation to the data in Table S2 we obtain values between 4% and 81%, with rates for solid tumors (the settings in which adaptive therapy has been most studied in) clustered below 25%. In light of this uncertainty, we choose to consider values of up to 50%. If turnover rates are higher this would simply further exaggerate our results. Future research should investigate turnover rates in tumors in more detail to obtain more accurate estimates.

S7 Indefinite Tumor Control

In order for a tumor to progress in our model it has to grow above 20% its initial size. However, the final size of the tumor under continuous therapy is limited by the so called "effective carrying capacity" of the resistant population, k_{Eff}. That is its steady state population density which is determined both by the environmental carrying capacity as well as the balance of birth to death rate. It is given by:

$$k_{\text{Eff}} = (1 - \hat{d}_R/\hat{r}_R) \tag{13}$$

Thus, if $k_{\text{Eff}} < 1.2n_0$ a tumor can not progress under continuous therapy nor adaptive therapy (for an example see Figures S8 A & B). This is a consequence of the simplifying assumption that the environmental carrying capacity, K, remains constant over time. In reality, the carrying capacity will expand over time due to angiogenesis and so the tumor would still eventually progress. As a result, the model behavior in this parameter domain is not representative of the underlying biology, and we did not consider these cases further. For discussion of a model which accounts for a dynamic carrying capacity due to angiogenesis during adaptive therapy, see [11] and [12].

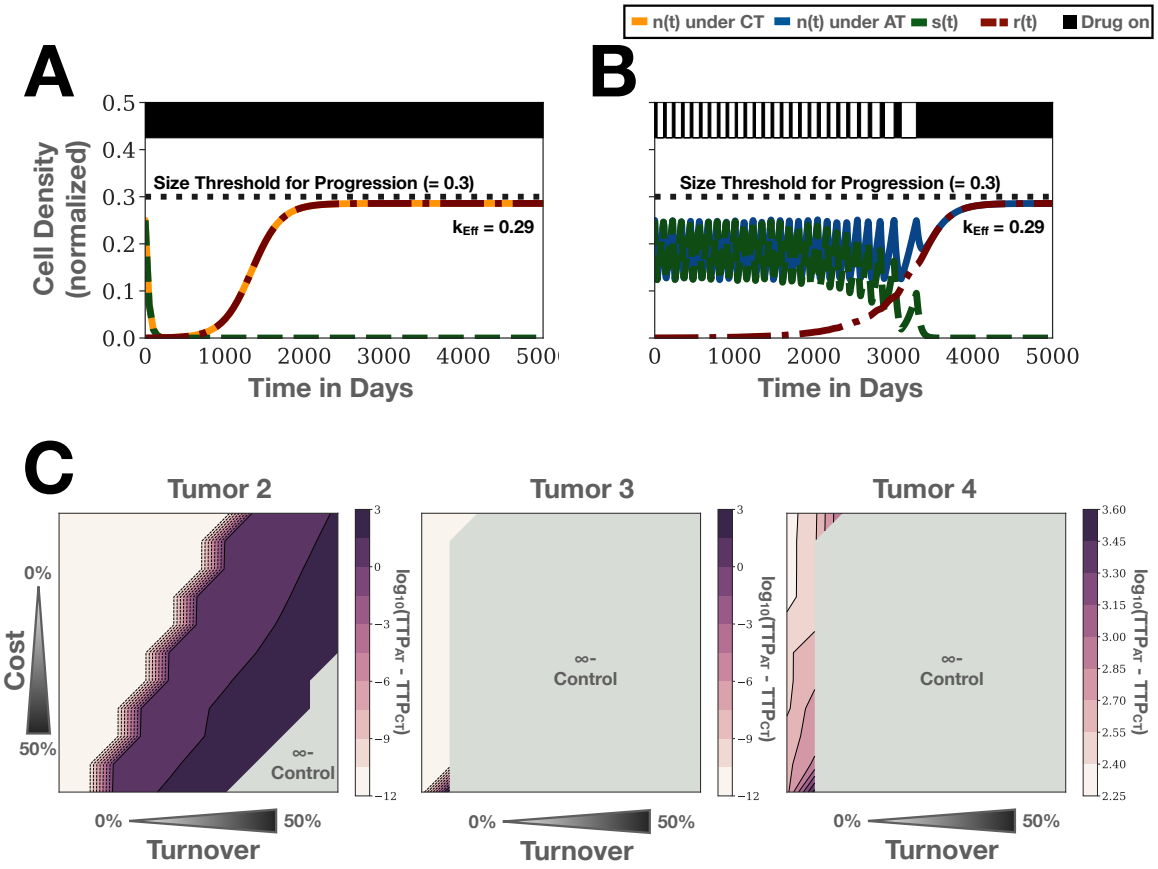

Figure S8: *As a consequence of the assumption that carrying capacity is constant the model allows for indefinite tumor control when* $(1 - \hat{d}_R/\hat{r}_R) < 1.2n_0$. *A: Example simulation illustrating indefinite control under continuous therapy for Tumor 1. While the tumor becomes completely resistant it can not grow above the 20% size increase required for progression, as the effective carrying capacity of the resistant population is too low. Parameters:* $n_0 = 25\%, f_R = 0.1\%, \hat{r}_R = 0.7, \hat{d}_R = 0.5$. *B: Same tumor as in A, but treated with adaptive therapy. Also in this case the tumor does not progress. C: The gain by adaptive therapy as a function of turnover and cost for Tumors 2-4. As Tumor 2 is far from carrying capacity* ($n_0 = 0.25$) *and has a high resistance portion, strong turnover and/or big resistance costs are required to see significant benefits of adaptive therapy. Conversely, since they are close to K* ($n_0 = 0.75$) *Tumors 3 & 4 are indefinitely controllable for a wide parameter regime.*

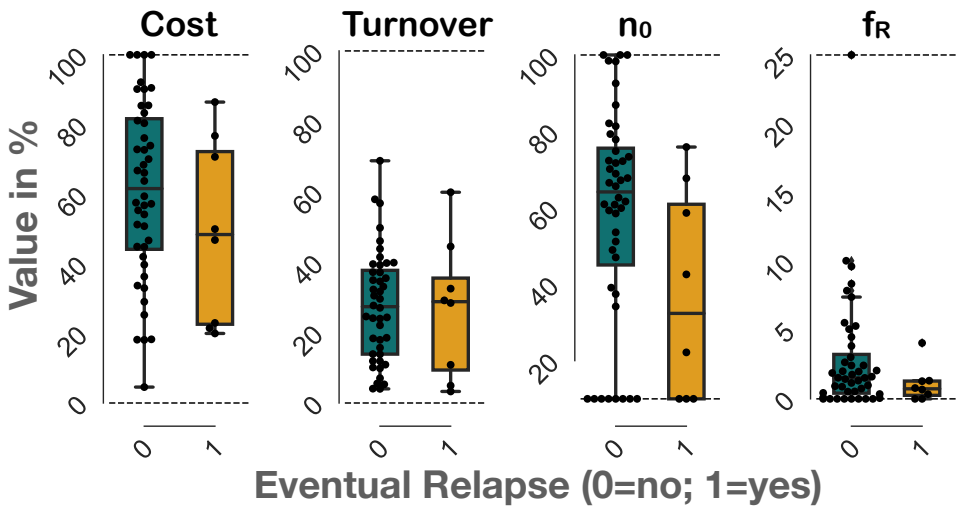

Figure S9: *Distribution of parameters obtained by fitting the model to each of 67 patients in the trial by Bruchovsky et al [13]. Dashed lines mark the limits imposed on the parameters during fitting. The only statistically significant difference is for the values of* n_0 *(Mann-Whitney U test, U=104.5, p-value* $= 3.5\%$*).*

References

[1] J. R. Dormand and P. J. Prince, "A family of embedded Runge-Kutta formulae," *Journal of Computational and Applied Mathematics*, vol. 6, no. 1, pp. 19–26, 1980.

[2] Y. Viossat and R. J. Noble, "The logic of containing tumors," *bioRxiv*, p. 2020.01.22.915355, jan 2020.

[3] J. A. Gallaher, P. M. Enriquez-Navas, K. A. Luddy, R. A. Gatenby, and A. R. Anderson, "Spatial heterogeneity and evolutionary dynamics modulate time to recurrence in continuous and adaptive cancer therapies," *Cancer Research*, vol. 78, no. 8, pp. 2127–2139, 2018.

[4] M. C. Lloyd, J. J. Cunningham, M. M. Bui, R. J. Gillies, J. S. Brown, and R. A. Gatenby, "Darwinian dynamics of intratumoral heterogeneity: Not solely random mutations but also variable environmental selection forces," *Cancer Research*, vol. 76, pp. 3136–3144, jun 2016.

[5] E. P. Malaise, N. Chavaudra, and M. Tubiana, "The relationship between growth rate, labelling index and histological type of human solid tumours," *European Journal of Cancer (1965)*, vol. 9, no. 4, pp. 305–312, 1973.

[6] G. G. Steel, K. Adams, and J. C. Barrett, "Analysis of the cell population kinetics of transplanted tumours of widely-differing growth rate," *British Journal of Cancer*, vol. 20, no. 4, pp. 784–800, 1966.

[7] G. G. Steel, "Cell loss as a factor in the growth rate of human tumours," *European Journal of Cancer (1965)*, vol. 3, no. 4-5, pp. 381–387, 1967.

[8] G. G. Steel, "CELL LOSS FROM EXPERIMENTAL TUMOURS," *Cell Proliferation*, vol. 1, no. 3, pp. 193–207, 1968.

[9] D. A. Rew and G. D. Wilson, "Cell production rates in human tissues and tumours and their significance. Part 1: An introduction to the techniques of measurement and their limitations," 2000.

[10] D. A. Rew and G. D. Wilson, "Cell production rates in human tissues and tumours and their significance. Part II: clinical data," 2000.

[11] R. A. Gatenby, A. S. Silva, R. J. Gillies, and B. R. Frieden, "Adaptive therapy," *Cancer Research*, vol. 69, pp. 4894–4903, jul 2009.

[12] K. Bacevic, R. Noble, A. Soffar, O. W. Ammar, B. Boszonyik, S. Prieto, C. Vincent, M. E. Hochberg, L. Krasinska, and D. Fisher, "Spatial competition constrains resistance to targeted cancer therapy," *Nature communications*, vol. 8, no. 1, pp. 1–15, 2017.

[13] N. Bruchovsky, L. Klotz, J. Crook, S. Malone, C. Ludgate, W. J. Morris, M. E. Gleave, and S. L. Goldenberg, "Final results of the Canadian prospective Phase II trial of intermittent androgen suppression for men in biochemical recurrence after radiotherapy for locally advanced prostate cancer: Clinical parameters," *Cancer*, vol. 107, pp. 389–395, jul 2006.